International Journal on
"Technical and Physical Problems of Engineering"
(IJTPE)
Published by International Organization of IOTPE

ISSN 2077-3528
IJTPE Journal
www.iotpe.com
ijtpe@iotpe.com

September 2024 | Issue 60 | Volume 16 | Number 3 | Pages 172-182

NUMERICAL INVESTIGATION OF MHD HYBRID NANOFLUID MIXED CONVECTION WITHIN A THREE-DIMENSIONAL L-SHAPED CAVITY

K. Bouzid [1] L. Belarche [1] B. Abourida [2] A. Siadi [1]

1. Laboratory of Mechanics, Processes, Energy and Environment, National School of Applied Science (ENSA), Ibn Zohr University, Agadir, Morocco, kamal.bouzid@edu.uiz.ac.ma, l.belarche@uiz.ac.ma, ali.siadi@edu.uiz.ac.ma
2. Laboratory of Fluid Mechanics and Energy, Faculty of Sciences, Cadi Ayyad University, Marrakesh, Morocco b.abourida@uiz.ac.ma

Abstract- The impact of magnetic field (H_a), cavity inclination (γ), particle volume fraction of Hybrid nanofluid (φ) on mixed convection within a three-dimensional L-shaped cavity filled with Hybrid nanofluids is numerically studied in this paper. The study's goal is to apprehend and optimize the impacts of all these selected parameters on the fluid pattern sand transfer of heat. The studied enclosure has a heated block in the west wall, and the Hybrid-nanofluids enter with a specific constant temperature to circulate in a part of the top wall. All the other parts of the enclosures are considered insulated. The Boussinesq approximation and the "FVA" are used to discretize and solve the equations that govern the model. Crucial thermal attitudes and fluid patterns are studied in terms of relevant parameters on isotherms, global Nusselt number, and streamlines. The findings suggest that increasing the Magnetic field intensity, and the volume fraction of hybrid particle enhance heat transfer. Conversely, increasing magnetic field inclination, except for γ=15° across all analyzed parameters, results in a decrease in heat transfer rate.

Keywords: Mixed Convection, Hybrid-Nanofluid, L-Shaped Cavity, Magnetic Field, Finite Volume Method, Hydrodynamic.

1. INTRODUCTION

Magneto-field and Hybrid nanofluid's properties in convection are employed in different domains where regular heat and mass transfer techniques struggle to provide optimum results. The use of hybrid nanofluids in "natural and mixed convection" has caught researchers' interest [1, 11] because to its extensive applications in both engineering technology and natural phenomena. The majority of industrial processes, including conditioning of nuclear reactors and electronic and mechanical components, drying technologies, and solar collectors.Another goal is to assist in the management of energy by researching potential improvements in thermal conductivity derived from a study of thermal efficiency and the factors influencing the thermophysical characteristics of the hybrid nanofluid.

To improve the convection rate in thesekinds of situations, a defined value of a magneto-field is implemented. Among the most important applications for this type of convection are tiny electronic devices and the thermal transfer required in reduced gravity equipment. A new research topic is the improvement of the heat transfer efficiency by creating an outside magnetic field, which is required for many industrial operrations. Hence, various heat transfer investigation projects have been completed, all with the target of developing novel strategies to improve thermal performance.

Fadaei, et al. [12] have investigated numericaly the impact of a magnetic field on the thermal conductivity propertiesof Fe_3-O_4 ferrofluids. The findings indicate that implementing a magnetic field increased the efficiency of transmission of heat, and the pace of improvement differed according to the degree of magnetic field force. Teamah [13] havestudied the consequence of the "M_f" intensity and heat source in an tending rectangular enclosure using multiple numerical simulations. The outcomes demonstrate that the presence of a "M_f" significantly influenced the flow patterns and heat transfer, and that when the Hartman number H_a>20, Over a wide range of R_a, the nusselt number and Sh keep constant.

Teamah, et al. [14] expanded their research by incorporating an inclined cavity into their investigation. The buoyancy force has been found to be more influenced by the angle of inclination in this study. Oztop, et al. [15] looked into the impact of a magnetic field on heat exchange by mixed convection in a cavity driven by a lid that contained a corner heater. In The computational simulations, they discovered that the magnetic field cause asignificant changes in the temperature and flow distribution, As a result, there was an augmentation in the rate of heat transmission. Hussain, et al. [16] relied on a numerical simulation to investigate the influence of the "M_f" on heat transmission in a wide cavity with a straight convey that included an adiabatic obstacle. The outcomes indicate that increasing R_i enhances heat transfer and increasing H_a improves Nusselt average.

Registered: 240225 Article Info: 1847 Accepted: 240825
Reserved: 240616 Available: 240930

Asadi, et al. [17] have conductedan analyzed study of laminar heat exchange in a channel through a sinusoidal ceiling submitted to a irregular "M_f". The study investigated the effect of differentes parameters such as magnetic field (intensity, direction), and wall geometry on the thermal efficiencyof the ferrofluid. It has been discovered that expanding the Hartman number, nanoparticle volume fraction, and "wave amplitude" enhance the rate of heat exchange. Kefayati's [18] study involved combining a lattice Boltzmann technique with a technique known as finite difference to replicate the impact of a magnetic fieldin a cavity triggered by the movement of two opposing lids. The findings indicated that the occurrence of a magnetic field causes aimportant improvement in the velocity of the blood flow, and that the magnetic field influences the blood's non-Newtonian behavior.

Aich, et al. [19] used computational fluid dynamics (CFD) to examine the buoyancy-driven airflow and generation of entropy in a 3D faceted greenhouse.The study aims to examinate the impact of various geometrical and operational parameters. In their study, The method of finite volumes (FVM) was used by the researchers to numerically resolve the mathematical models of heat Transfer alongside fluid behavior. The outcomes indicate that the greenhouse's height and the opening area significantly affect the natural airflowand entropy generation. Al Salem, et al. [20] evaluated the impact of changing the lid orientation under magneto-hydro-dynamic in a gradually heated hollow. The results demonstrate that the orientation of the lid motion has a significant influence on the flow patterns and heat eficiencerates, and that raising the magnetic field strenghtreduce the heat eficience rate for all various parameters. Ghorbanietal [21] have presented a computational fluid dynamics (CFD) study and compassion analysis on heat transfer improvement of Fe_3O_4-water ferrofluid flow submitted to a magnetic field. The findings demonstrate that the intensity of field-magnetic has a crucial impact on heat transfer enhancement, while the effects of fluidvolume fraction is less significant. Amgharani, et al. [22] have performed a computational simulation of mixed convection to examines the hydrodynamic and magnetic field effects within an 2D L enclosure full with hybrid nano-fluid (Al_2O_3-Cu water), with a localized heat source/sink. Based on the obtained results the Nusselt number and entropy formation are influenced by the magnetic field angle in a sinusoidal manner. The angles of 60 and 240 degrees yield the maximum magnetic field strength, resulting in the most effective influence.

Additionally, for optimal heat transfer performance, an angle of 180 degrees is found to be the best choice for the magnetic field. Mehrez and Cafsi [23] have executed numerical simulations to examine and analyze the impact of varying the intensity of "M_f" and non-uniformity on the movement and temperature exchange characteristics of the nano-fluid. The results examinate that the non-uniform magnetic field strengthen the rate of heat exchange, while the uniform field of magnets has no influence on the heat exchange rate. Despite the extensive research conducted on this topic to understand the phenomenon of "mixed convection" in enclosures with multiples designs and boundary conditions, there is a notable scarcity of research specifically examining the situation of mixed convection occurring in an L-shaped cavity. This particular scenario involves an L-shaped cavity with a heated block placed inside, and the cavity is further exposed to the impact of a "M_f".

Although the significance of "mixed convection" in practical areas, including heat transfer systems and thermal management, there remains a gap in understanding the intricate dynamics occurring within L-shaped cavities under the combined effects of mixed convection, heating block, and magnetic fields. Exploring this unique configuration can provide valuable insights into the transfer of heat and fluid behaviors in complex geometries, contributing to the advancement of engineering concept and improvement in various fields.

2. PROBLEM FORMULATION

This study focuses on numerically investigating mixed convection of a Hybrid-nanofluids (water with suspended Cu/Al_2O_3 Nano elements) in a 3D L-shaped cavity with a heating block submitted to magneto-fields. As illustrated in Figure 1, the configuration size is $H \times 3H$ for each element. The hybrid nanofluid enters the cavity via an upper wall section with an inlet temperature Tc and velocity Vin, and then exits through a section below the right wall with (w=H/4). An heated block with (b=H/3 and a=w/2) is positioned on the left wall with (h = H/3), and in the middle of the cavity with (l = H/2). All the others walls are considered insulated.

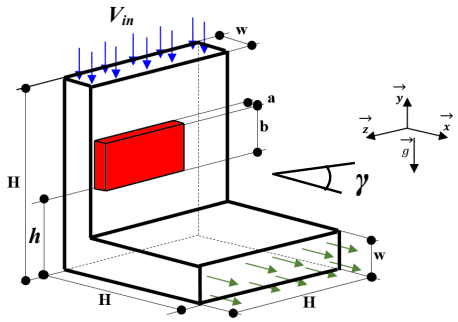

Figure 1. Studied configuration and co-ordinates

3. NUMERICAL SCHEME AND MATHEMATICAL MODELLING

The configuration of the current study is a 3D-L cavity filled with (Al_2O_3-Cu) combined with water (hybrid-nano-fluid) under buoyancy force, as shown in Figure 1. Magneto-fields have an angle of γ. The L-shaped cavity's walls are all adiabatics, and an heated obstacle is situated in the left wall. It is assumed that the flow is laminar, three-dimensional, and steady, and that the based hybrid-nanofluid is Newtonian and incompressible; radiation effects are ignored. Table 1 presents the characteristics of nanoparticles and base fluid.

Table 1. Properties of hybrid-nanofluids [27]

Property	Alumina (Al_2O_3)	Water	Copper (Cu)
β (K^{-1})	0.85×10^{-5}	21×10^{-5}	1.67×10^{-5}
ρ ($kg\times m^{-3}$)	3970	997.1	8933
σ ($\Omega\times m^{-1}$)	2.7×10^{-8}	5.5×10^{-6}	5.96×10^{-7}
k ($W\times m^{-1}\times K^{-1}$)	40	0.613	401
C_p ($J\times kg^{-1}\times K^{-1}$)	765	4179	385

The Boussinesq approximation is used to estimate density variations. Based on these assumptions, the prevailing equations can be written as [22]:

$$\frac{\partial u}{\partial x}+\frac{\partial w}{\partial z}+\frac{\partial v}{\partial y}=0 \tag{1}$$

$$\frac{\partial(uu)}{\partial x}+\frac{\partial(vu)}{\partial y}+\frac{\partial(wu)}{\partial z}=v_{Hnf}\left(\frac{\partial^2 u}{\partial x^2}+\frac{\partial^2 u}{\partial y^2}+\frac{\partial^2 u}{\partial z^2}\right)- -\frac{1}{\rho_{Hnf}}\frac{\partial p}{\partial x}+\frac{\sigma_n B_0^2}{\rho_{Hnf}}(v\sin\gamma\cos\gamma-u\sin^2\gamma) \tag{2}$$

$$\frac{\partial(uv)}{\partial x}+\frac{\partial(vv)}{\partial y}+\frac{\partial(wv)}{\partial z}=-\frac{1}{\rho_{Hnf}}\frac{\partial p}{\partial y}+ +\frac{\sigma_n B_0^2}{\rho_{Hnf}}(u\sin\gamma\cos\gamma-v\cos^2\gamma)+ +v_{Hnf}\left(\frac{\partial^2 v}{\partial x^2}+\frac{\partial^2 v}{\partial y^2}+\frac{\partial^2 v}{\partial z^2}\right)+\frac{(\rho\beta)_{Hnf}}{\rho_{Hnf}}g(T=T_{ref}) \tag{3}$$

$$\frac{\partial(uw)}{\partial x}+\frac{\partial(vw)}{\partial y}+\frac{\partial(ww)}{\partial z}=-\frac{1}{\rho_{Hnf}}\frac{\partial p}{\partial z}+ +v_{Hnf}\left(\frac{\partial^2 w}{\partial x^2}+\frac{\partial^2 w}{\partial y^2}+\frac{\partial^2 w}{\partial z^2}\right) \tag{4}$$

$$\frac{\partial(uT)}{\partial x}+\frac{\partial(vT)}{\partial y}+\frac{\partial(wT)}{\partial z}=\frac{Q_0}{(\rho c_p)_{Hnf}}(T=T_{ref})+ +\alpha_{Hnf}\left(\frac{\partial^2 T}{\partial x^2}+\frac{\partial^2 T}{\partial y^2}+\frac{\partial^2 T}{\partial z^2}\right) \tag{5}$$

The boundary conditions are:

- At the outlet: $\frac{\partial u}{\partial x}=0$; $\frac{\partial v}{\partial y}=0$; $\frac{\partial w}{\partial z}=0$; $\frac{\partial T}{\partial n}=0$
- At the creek: $v=v_{in}$; $u=w=0$; $T=T_C$

On the remaining walls: u=v=w=0, $\frac{\partial T}{\partial n'}=0$, where n' represents the normal direction perpendicular to the respective wall under consideration. At the block: $\frac{\partial T}{\partial m'}=-\frac{q''}{K_{Hnf}}$; u=v=w=0; (m' refers to the normal direction perpendicular to the block wall). The properties of the hybrid-nanofluid are specified by the subsequent equations [22]:

The density formula of the hybrid nanofluid is defined as:

$$\rho_{Hnf}=\varphi_{p1}\rho_{p1}+\varphi_{p2}\rho_{p2}+(1-\varphi)\rho_f \tag{6}$$

The concentration of the nanoparticles is described as:

$$\varphi=\varphi_{p1}+\varphi_{p2} \tag{7}$$

The heat capacitance is calculate as:

$$(\rho C_p)_{Hnf}=\varphi_{p1}(\rho C_p)_{p1}+\varphi_{p2}(\rho C_p)_{p2}+(1-\varphi)(\rho C_p)_f \tag{8}$$

The thermal coefficient expansionis identified as:

$$(\rho\beta)_{Hnf}=\varphi_{p1}(\rho\beta)_{p1}+\varphi_{p2}(\rho\beta)_{p2}+(1-\varphi)(\rho\beta)_f \tag{9}$$

The expression for thermal diffusivity in hybrid nanofluids takes the following form:

$$\alpha_{Hnf}=K_{Hnf}/(\rho Cp)_{Hnf} \tag{10}$$

Determination of the thermal conductivity as follows:

$$\frac{K_{Hnf}}{K_f}=\frac{\frac{(\varphi_{p1}K_{p1}+\varphi_{p2}K_{p2})}{\varphi}+2K_f+2(\varphi_{p1}K_{p1}+K_{p2}\varphi_{p2})-2K_f\varphi}{\frac{(\varphi_{p1}K_{p1}+K_{p2}\varphi_{p2})}{\varphi}-(\varphi_{p1}K_{p1}+K_{p2}\varphi_{p2})+2K_f+K_f\varphi} \tag{11}$$

Hybrid nanofluid with the following dynamic viscosity:

$$\alpha_{Hnf}=\mu_f/[1-(\varphi_{p1}-\varphi_{p2})^{2.5}] \tag{12}$$

The effective electrical conductivity is expressed as:

$$\frac{\sigma_{Hnf}}{\sigma_f}=\frac{3(\frac{(\varphi_{p1}\sigma_{p1}+\varphi_{p2}\sigma_{p2})}{\sigma_f}-\varphi_p)}{(\frac{(\varphi_{p2}\sigma_{p2}+\sigma_{p1}\varphi_{p1})}{\varphi\sigma_f}+2)-(\frac{(\varphi_{p2}\sigma_{p2}+\sigma_{p1}\varphi_{p1})}{\varphi\sigma_f}-\varphi_p)} \tag{13}$$

By identifying the boundaries:

$$X=\frac{x}{H},\ Z=\frac{z}{H},\ Y=\frac{y}{H},\ U=\frac{u}{V_{in}},\ W=\frac{w}{V_{in}},\ V=\frac{v}{V_{in}}$$

$$R_i=\frac{G_r}{R_e^2},\ \theta=\frac{(T-TC)}{q''H}K_{Hnf},\ P=\frac{p}{\rho_{Hnf}V_{in}{}^2} \tag{14}$$

The governing equations are transformed into dimensionless equations, which are presented as follows:

$$\frac{\partial U}{\partial X}+\frac{\partial W}{\partial z}+\frac{\partial V}{\partial Y}=0 \tag{15}$$

$$U\frac{\partial(U)}{\partial X}+U\frac{\partial(W)}{\partial Z}+U\frac{\partial(V)}{\partial Y}=-\frac{\partial P}{\partial X}+ +\frac{1}{R_e}\left(\frac{v_{Hnf}}{v_f}\right)\left(\frac{\partial^2 U}{\partial X^2}+\frac{\partial^2 U}{\partial Y^2}+\frac{\partial^2 U}{\partial Z^2}\right)+ +\left(\frac{\sigma_{Hnf}\rho_f}{\sigma_f\rho_{Hnf}}\right)\frac{H_a^2}{R_e}(V\sin\gamma\cos\gamma-U\sin^2\gamma) \tag{16}$$

$$V\frac{\partial(U)}{\partial X}+V\frac{\partial(W)}{\partial Z}+V\frac{\partial(V)}{\partial Y}=-\frac{\partial P}{\partial Y}+R_i\frac{(\rho\beta)_{Hnf}}{\rho_{nf}\beta_f}\theta+ +\frac{1}{R_e}\left(\frac{v_{Hnf}}{v_f}\right)\left(\frac{\partial^2 V}{\partial X^2}+\frac{\partial^2 V}{\partial Y^2}+\frac{\partial^2 V}{\partial Z^2}\right)+ +\left(\frac{\sigma_{Hnf}\rho_f}{\sigma_f\rho_{Hnf}}\right)\frac{H_a^2}{R_e}(U\sin\gamma\cos\gamma-V\cos^2\gamma) \tag{17}$$

$$W\frac{\partial(U)}{\partial X}+W\frac{\partial(V)}{\partial Y}+W\frac{\partial(W)}{\partial Z}=-\frac{\partial P}{\partial Z}+ +\frac{1}{R_e}\left(\frac{v_{Hnf}}{v_f}\right)\left(\frac{\partial^2 W}{\partial X^2}+\frac{\partial^2 W}{\partial Y^2}+\frac{\partial^2 W}{\partial Z^2}\right) \tag{18}$$

$$U\frac{\partial\theta}{\partial X}+W\frac{\partial\theta}{\partial Z}+V\frac{\partial\theta}{\partial Y}=\frac{(\rho c_p)_f}{(\rho c_p)_{Hnf}}\left(\frac{1}{RePr}\right)Q\theta+ +\left(\frac{\alpha_{Hnf}}{\alpha_f}\right)\left(\frac{1}{R_eP_r}\right)\left(\frac{\partial^2\theta}{\partial X^2}+\frac{\partial^2\theta}{\partial Y^2}+\frac{\partial^2\theta}{\partial Z^2}\right) \tag{19}$$

where, $G_r = \frac{g\beta_f H^3 \Delta T}{vf^2}$, $H_a = B_0 H\sqrt{\frac{\sigma_f}{\mu_f}}$, $P_r = \frac{v_f}{\alpha_f}$ and $R_e = \frac{V_{in} H}{v_f}$ are successively Grashof, Hartman, Prandtl and Reynolds numbers.

The following is an outline of the dimensionless boundaries :

- At the outlet: $\frac{\partial U}{\partial X} = 0$; $\frac{\partial V}{\partial Y} = 0$; $\frac{\partial W}{\partial Z} = 0$; $\frac{\partial T}{\partial n} = 0$
- At the inlet: $V = V_{in}$; $U = W = 0$; $\theta = 0$

On the remaining walls: $U = V = W = 0$; $\frac{\partial \theta}{\partial n'} = 0$ (n' represents the conventional direction normal to the measured wall);

At the block: $\frac{\partial \theta}{\partial m'} = -\frac{K_{Hnf}}{K_f}$, u=v=w=0, where m' refers to the perpendicular direction to the block wall. The Nusselt number is determined depending on the situation under consideration:

The local Nusselt number is calculated for sections (S_i) with (i varies from 1 to 5) as follows:

$$NU_{S1} = \frac{q''H}{[T(x,z)_{y=h} - T_C]k} = \frac{1}{\theta(X,Z)_{Y=h}}$$

$$NU_{S2} = \frac{q''H}{[T(x,z)_{y=h+b} - T_C]k} = \frac{1}{\theta(X,Z)_{Y=h+B}}$$

$$NU_{S3} = \frac{q''H}{[T(y,z)_{x=a} - T_C]k} = \frac{1}{\theta(Y,Z)_{X=A}} \quad (20)$$

$$NU_{S4} = \frac{q''H}{[T(x,y)_{z=H/4} - T_C]k} = \frac{1}{\theta(X,Y)_{Z=H/4}}$$

$$NU_{S5} = \frac{q''H}{[T(x,y)_{y=3H/4} - T_C]k} = \frac{1}{\theta(X,Y)_{Z=3H/4}}$$

The global Nusselt number can be described as:

$$NU_G = NU_{SG1} + NU_{SG2} + NU_{SG3} + NU_{SG4} + NU_{SG5} \quad (21)$$

The global Nusselt numbers for each section, represented as NUSGi, are provided as follows:

$$NU_{SG1} = \frac{2}{A \times H} \int_{H/4}^{3H/4} \int_{0}^{A} NU_{S1} dXdZ$$

$$NU_{SG2} = \frac{2}{A \times H} \int_{H/4}^{3H/4} \int_{0}^{A} NU_{S2} dXdZ$$

$$NU_{SG3} = \frac{2}{B \times H} \int_{0}^{B} \int_{H/4}^{3H/4} NU_{S3} dYdZ \quad (22)$$

$$NU_{SG4} = \frac{1}{B \times A} \int_{h}^{h+B} \int_{0}^{A} NU_{S4} dYdX$$

$$NU_{SG5} = \frac{1}{B \times A} \int_{h}^{h+B} \int_{0}^{A} NU_{S5} dYdX$$

4. NUMERICAL METHOD

Toresolve the system of Equations (15)-(19) with their associated boundary conditions, a computational Fortran home program has been established.. The program uses the finite volume approach and employs the power-law scheme as proposed by Patankar [24]. To link the pressure and velocity fields, the program implements the SIMPLEC algorithm, originally proposed by Van Doormaal and Raithby in 1984. This algorithm effectively handles the interaction between pressure and velocity, ensuring accurate and consistent results.

To resolve the consequent system of mathematical equations, the tri-diagonal matrix approach, developed by Thomas, is employed. This algorithm is applied incrementally, solving the equations line by line in an iterative manner. By employing this approach, the program achieves efficient and reliable resolution of the algebraic equations system. During the iterative process, program continuously monitors the residuals of stream function. The residuals' convergence criterion is set to 10^{-5}. Once the residuals drop below this threshold, indicating that the solution has sufficiently converged, the numerical code is considered to have reached convergence.

4.1. Grid Size Independency

The selection of an appropriate grid size is crucial in computational simulations as it affects the accuracy and computational resources required. To accomplish the solution's grid independence, the Nusselt number was evaluated using various uniform grid sizes. The findings are displayed in Table 2. Considering the analysis, the 81×81×81 grid was found to be compatible with the current study, as it gives a equilibrium between the precision of the results and the numerically cost.

Furthermore, when the grid was refined to 91^3, the extreme difference remained within 1.18%. This suggests that the adjusted grid size had no major effect on the general functioning of the system, promoting the appropriateness of the 81^3 grid for the purpose of the research.The results of this investigation verify the implementation of the selected grid size while offering trust in the accuracy of the outcomes achieved while improving the effectiveness of computation.

Table 2. Grid size tests

Grid Size	41×41×41	61×61×61	71×71×71	81×81×81	91×91×91
Nusselt Number	44.18	55.28	58.99	59.40	60.11

4.2. Code Validation

To verify the reliability of our computational code, we compared the Nusselt numbers that resulted from the simulations we performed to those provided in earlier research by Ravnik [25], Doghmi, et al. [28] and Moraga, et al. [26]. The findings of the analysis are summed up in Tables 3 and 4, in which distinctive Rayleigh numbers were taken into account. Likewise, as can be seen in Figure 2, we juxtaposed the thermal distribution acquired from our modeling techniques to the findings provided by Doghmi, et al. [28].

In Comparison between our findings and those of earlier research Ravnik [25], Moraga, et al. [26] and Doghmi, et al. [28] reveal a high level of approval, with an overall variance of roughly 3.24%. This suggests that our numerical algorithm effectively replicates the key features of the issue and creates outcomes that are compatible with developed literary works.

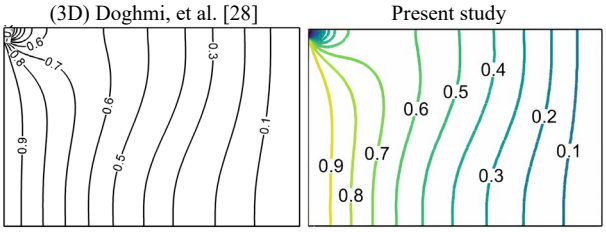

Figure 2. Comparison of isotherm when R_e=10 and R_i=10 with ref. [28]

Table 3. Comparison of Nusselt number with those of Ravnik [25]

Ra	Water		Gap%	(Water + Cu) φ= 0.1		Gap%
	Present work	Ref. Ravnik [25]		Present work	Ref. Ravnik [25]	
10^3	1.082	1.071	1.02%	1.381	1.363	1.32%
10^4	2.114	2.078	1.73%	2.257	2.237	0.89%
10^5	4.631	4.510	2.68%	5.047	4.946	2.04%
10^6	9.325	9.032	3.24%	10.38	10.08	2.97%

Table 4. Comparison of Nusselt number with those of ref. [26]

R_e	R_i=0		Gap%	R_i=0.1		Gap%
	Present work	Moraga, et al. [26]		Present work	Moraga, et al. [26]	
10	2.550	2.552	0.07%	2.550	2.552	0.07%
50	3.517	3.512	0.14%	3.509	3.500	0.25%
80	4.127	4.122	0.12%	4.120	4.077	1.05%
300	5.102	5.084	0.35%	5.814	5.706	1.89%
500	5.605	5.567	0.68%	7.351	7.157	2.71%

5. RESULTS AND DISCUSSION

The primary goal of this study is to look at how dimensional and thermal factors affect fluid flow behaviors and heat exchange inside a three-dimensional L-shaped hollow. The research emphasizes on multiple important features, such as variation in temperature, global Nusselt number, fluid structures, and streamlines. To accomplish this, multiple thermal characteristics are taken into account, includingthe Hartman numbers ($0 \le H_a \le 100$), Reynolds numbers ($10 \le R_e \le 1900$), magnetic field inclination ($0 \le \gamma \le 45$), and volume fraction of nanoparticles ($0\% \le \varphi \le 4\%$).

5.1. Effect of the Thermal Parameters

Figure 3 depicts an analysis of the isotherms in various layers for the examined setting up. Particularly, when viewed from the plane Z=0.5, the cavity exhibits an advantageous level of symmetry. This symmetry is due to thermal borders and the configuration's related geometrical symmetry. The Z=0.5 plane has the most behavior of the planes studied, making it especially suited for displaying and evaluating the dynamical and thermal fields inside the examinatedcavity. By focusing on this plane, we can gain a detailed understanding of the complex fluid flow patterns and temperature dispersion in the system.

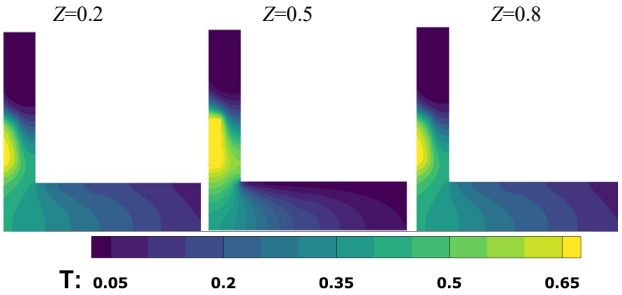

Figure 3. Temperature distribution for various Z positions (0.2, 0.5 and 0.8), for R_e=100, R_i=0.1 and φ=3%

Figure 4 illustrates the impact of the Reynolds numbers and fractional volume of Hybrid-nanoparticles on 3-D flow layout and temperature variation within the L-shaped cavity for an invariant setting of Hartman number H_a=10, Richardson number R_i=0.1, and magnetic field angle of inclination γ=0°. By considering the entrance boundary conditions, the velocity behavior, and examining two cases with volume fractions of Hybrid-nanoparticles (φ) set at 2% and 4%, it becomes evident that enhancing the Reynolds number has a substantial positive impact on heat transfer.

The Reynolds number reflects the ratio of inertial to viscous forces, indicating a direct relationship between velocity and Reynolds number. As a result, when the Reynolds number increases, heat transfer improves significantly. With the presence of a left-side obstacle (heated block),the viscous fluid's velocity forms a tiny clockwise vortex at the bottom of the block. However, this clockwise vortex diminishes as the Reynolds number increases, particularly reaching a moderate value of R_e=500. The association of metal nanoparticles with the base fluid is critical in this phenomenon.

The presence of the nanoparticles alters the fluid's density and particle mobility, leading to changes in flow characteristics.Furthermore, for Reynolds numbers $R_e \ge 500$, excellent heat transfer is observed due to aimportant iincrease in the fluid velocity. This occurs when a balance is achieved between the inertial forces and the characteristics of the nanoparticles.

Moreover, in this study, It has been observed that raising the volume fraction of Hybrid nanofluid particles leads to an enhancement in heat transfer, except for cases where the Reynolds number $R_e \le 100$. Physically, in the studied configuration, heat transfer occurs as the temperature moves from the hot body (heated block) to the cold body (incoming fluid). As a result, the temperature distribution gradually spreadtoward the heated block and progressively shifts around the hollowexit.This phenomenon arises from the exhangewithing the oncoming cold fluid and the buoyancy effect of the heated block. Furthermore, for Reynolds numbers $R_e \le 100$, the temperature distribution reveals that increasing the volume fraction (φ) diminishes heat transfer. In these cases, the higher volume fraction of nanoparticles lowers heat transfer rather than enhancing it.

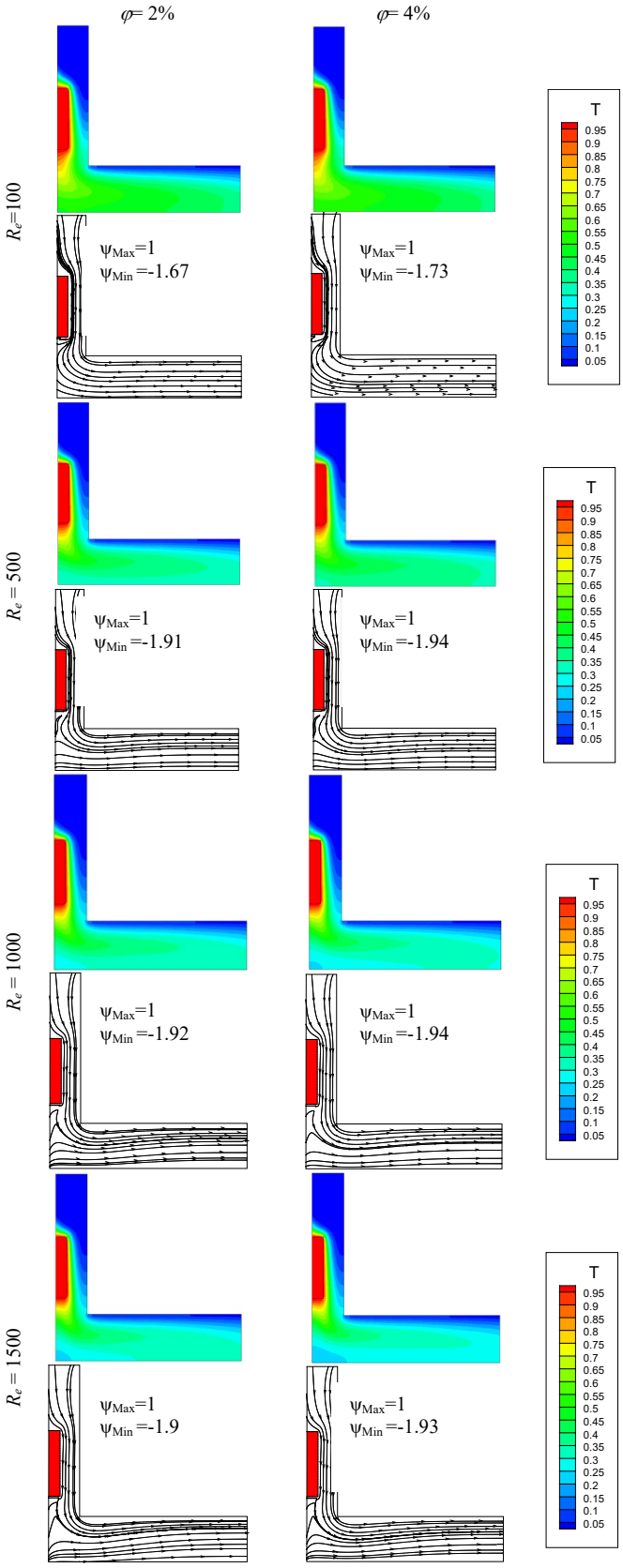

Figure 4. Isotherm lines (up) and streamlines (down), for H_a=10, for R_i=0.1, for γ=0° and for various Reynold numbers (100, 500, 1000 and 1500), and for differents values of Hybrid nanoparticles φ=2% and φ=4%

Figure 5 presents the hydrodynamical and thermal fields, aiming to highlight the impact of the Hartman numbers and the Hybrid-nanoparticles volume fraction on the 3-D flow arrangement and temperature exhange inside the L-shaped cavity. This investigation is conducted while maintaining a constant value of the Reynolds number R_e at 750, Richardson number Ri at 0.1, and magnetic field angle of inclination γ at 0°. the results analyzed the impact of the Hartmann number on the fluid dynamics. The velocity was oriented from top to bottom.

In this study, the fluid being investigated was electrically conducting, and the effect of the Lorentz force improved the fluid flow, leading to an augmentation in the velocity field.This improved fluid mixing lead to a more uniform temperature distribution throughout the system, and more efficience heat, reducing temperature gradients and minimizing the hot temperature arround the block spots. When the Hartmann number reached H_a=100, a direct association between H_a and fluid velocity was observed for all values of φ. Specifically, as the H_a value increased, the fluid velocity showed a significant increase as well.In addition to the changes in velocity, It became apparent that as the Ha values increased, the boundary layering expanded. Figure 5 shows the effect of "M_f" inclination (γ) on temperature exhange and fluid contours under a variety of Hartmann numbers (H_a) (ranging from H_a=10 to H_a=100).

The velocity profile shows a decrease as the inclination angle γ increases. Morever, Figure. 6 is depicted to evaluate the influence of φ on fluid patterns and temperature distribution for two cases of Hartman number H_a=10 and H_a=100. It has been found that increasing (φ) for a set value of Ha has a negligible effect on temperature patters and a sustainable impact on velocity profile. Initially, for H_a =10, the temperature is more toward the left block for differentes values of (φ), and by increasing the Hartman number to H_a=100, the temperature expand in the cavity.

5.2. Global Nusselt Number

Figure 7 illustrates the results obtained for various values of Reynold number (R_e ranged from 50 to 1900) and Magnetic field intensity (H_a ranged from 10 to 100) for fixed values of Richardson number (R_i=0.1), particle volume fraction (φ=4%), and magnetic field inclination (γ=0°) in form of global Nusselt number in the heated block. The results demonstrated that increasing Reynolds number increase the global nusselt , wish can be explained as the Reynolds number reflects the balance inertia and viscous forces.

Additionally, when increasing the magnetic field intensity, the global nussel number increases for all Reynolds numbers except for R_e=200, and H_a=100, where the heat transfert has diminished. Likewise, the variations in global Nusselt numbers between Reynolds numbers R_e=700 and R_e=1900 are less than 1%.

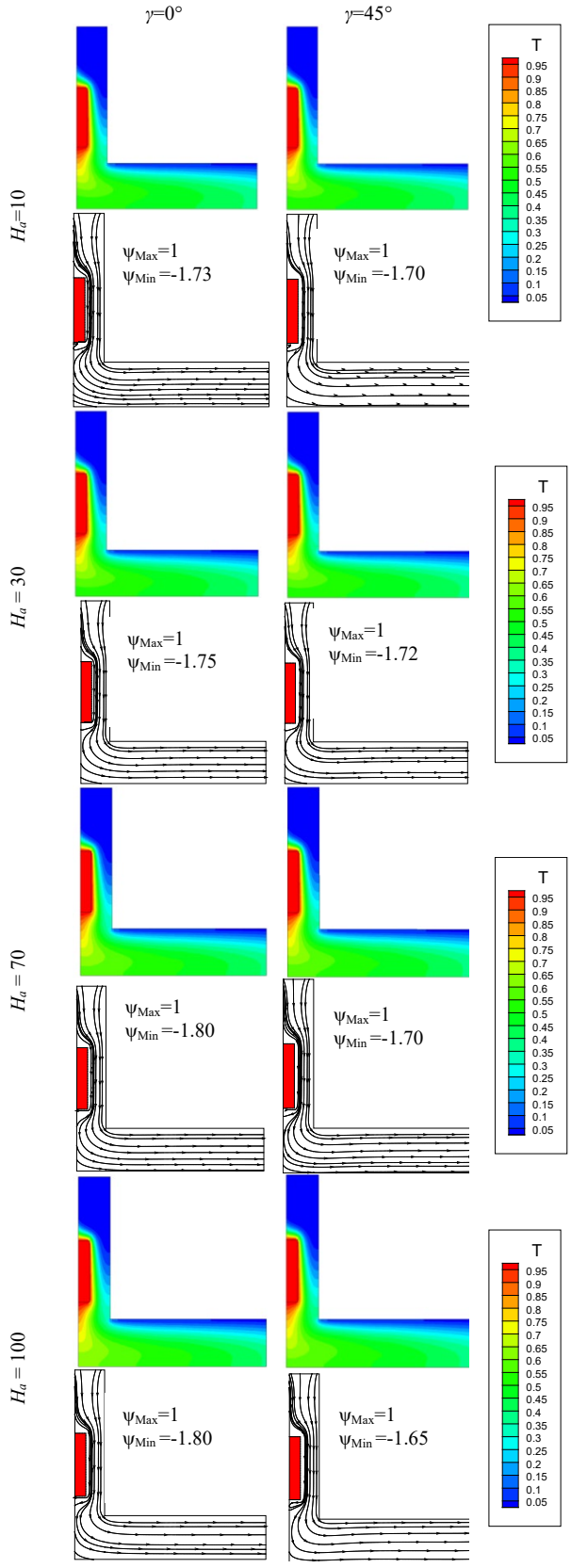

Figure 5. Isotherm lines (up) and streamlines (down), for R_e=100, for φ=4%, for R_i = 0.1, and for for various Hartman number H_a (10, 30, 70 and100), for differents values of angles of inclinaison γ=0° and γ=45°

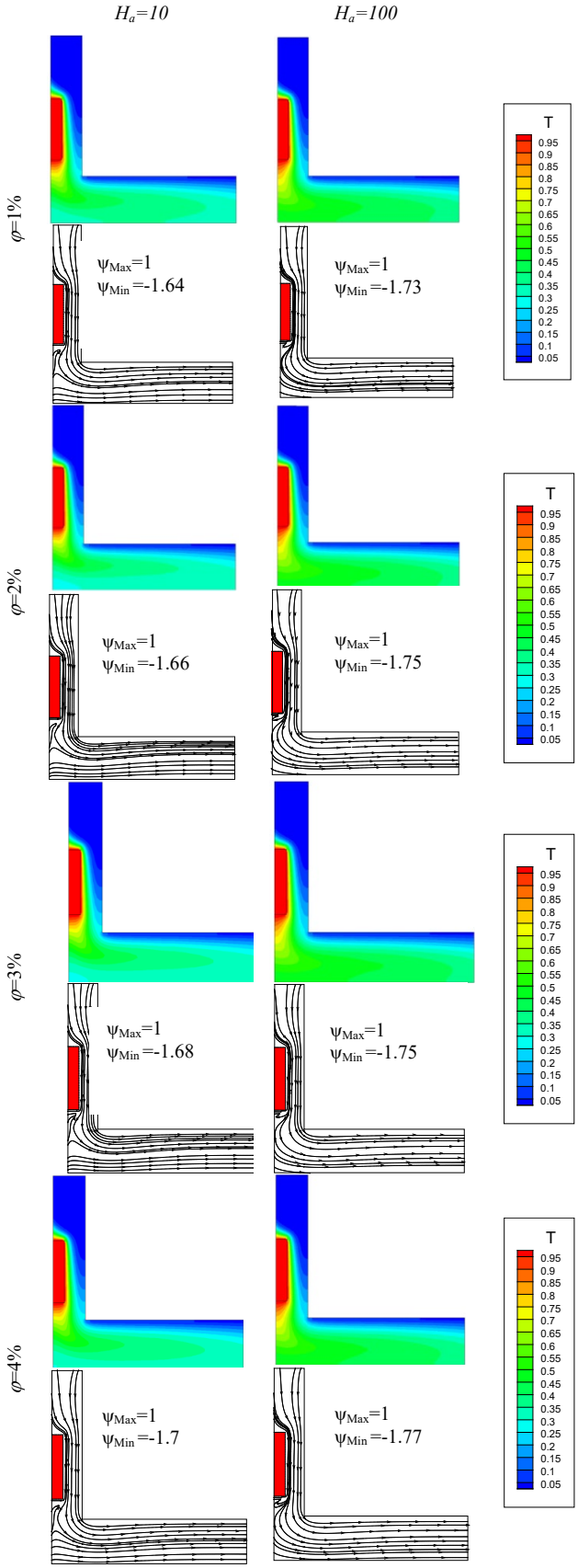

Figure 6. Isotherm lines (up) and streamlines (down), for γ=0°, for R_e=750, for R_i=0.1, and for for various Hybrid nanoparticles volume (1%, 2%, 3% and 4%), for differents values of Hartman number H_a=0 and H_a=100

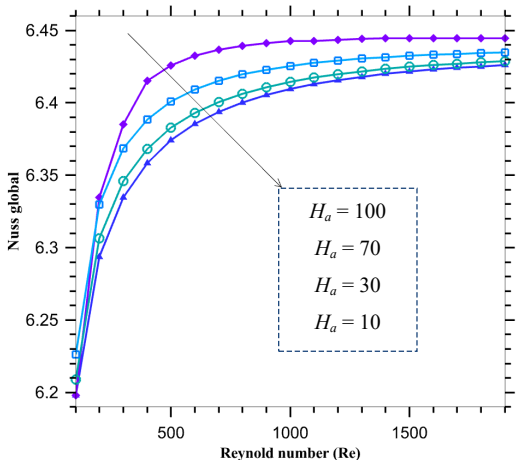

Figure 7. The global Nusselt number variation with R_e, for φ=4%, R_i=0.1, and γ=0°, and for different values of H_a (10, 40, 70, and 100)

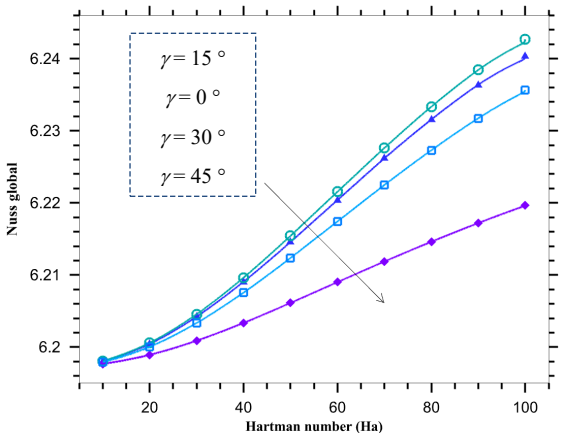

Figure 8. The global Nusselt number variation with H_a, for φ=4%, R_i=0.1, and R_e=100,andfor different values of γ (0°, 15°, 30°, and 45°)

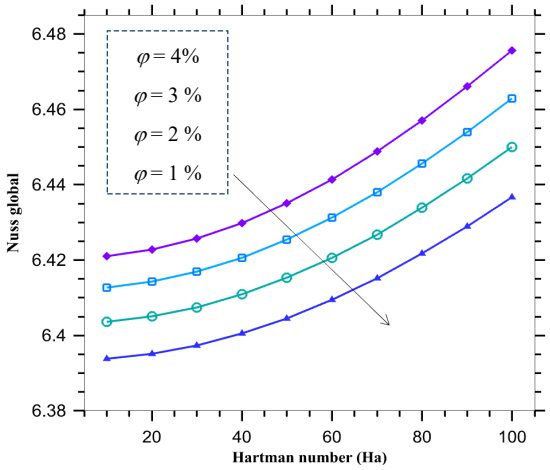

Figure 9. The global Nusselt number variation with H_a, for R_e=700, R_i=0.1, and γ=0°, and for different values of φ (1%, 2%, 3%, and 4%)

This behavior has been observed for all the considered Hartman numbers. Based on the results displayed in Figure 8, the Heat transfer enhances as the Hartman number (H_a) and angle of inclination (γ) increase, except for the case where the angle of inclination (γ) is set to 15°, the effect remains unchanged for a fixed parameters such as R_i=0.1, φ=4%, and R_e=100.

The highest values for the global Nusselt number are obtained in this case. The results can be summarized that increasing the magnetic field intensity (H_a) has a more pronounced impact on enhancing heat transfer compared to decreasing the inclination angle (γ).

Furthermore, for certain values of inclination (in this case, γ=15°), the enhancement in heat transfer becomes particularly noticeable. This result can be explained by the reality that expanding the Hartman number (H_a) enhances the velocity profile, thereby promoting inertia and the Lorenz force within the cavity. In Figure 9, the influence of increasing the the hybrid nanofluid volume fraction on the overall Nusselt number is depicted while maintaining a constant Reynolds number (R_e=700), inclination of angle (γ=0°), and Richardson number (R_i=0.1). The graph reveals that as (φ) increases, overall Nusselt number alsoenhances. Furthermore, Figure 9 shows that increasing Hartman number leads to enhanced heat transfer for all nanoparticle volume fraction.

These results indicate that higher volume fractions of the hybrid nanofluid and stronger magnetic fields contribute to elevated heat transfer rates, ultimately improving the efficiency of the system.

6. CONLUSIONS

The primary goal of this investigation is to optimize important variables such as the Hartman number, Reynolds number, particle volume fraction, and magnetic field inclination on mixed convection of an *H*. nanofluid's inside an L-shaped enclosure containing a heated block. To accomplish this goal, a diverse set of parameters are chosen and their effect on the intended result is evaluated. The Hartman number ($10 \le H_a \le 100$), magnetic field inclination angle angle ($0° \le \gamma \le 45°$),volume fraction of hybrid nanoparticles ($1\% \le \varphi \le 4\%$), and Reynolds number ($10 \le R_e \le 1900$) were all chosen as computational conditions for this study. Throughout the investigation, the dimensions of the heated block and the Richardson number (R_i=0.1) are considered constant. The investigation's outcomes indicate that the parameters mentioned earlier have significant effects on both the velocity field and the heat transfer behaviors. The main insights are summed up below:

- The volume fraction of particles and the Hartman number have an important effect on thermal field and flow structures.
- Except for γ=15°, fluid flow increases with increasing magnetic strength and nanoparticle concentration, while it decreases with rising magnetic field inclination.
- The temperature distribution is less affected by an enhance in inclination of magnetic field and nanoparticles volume fraction for a set value of H_a than an increase in Hartman number for a fixed value of φ and γ.
- This analysis takes into account multiple Reynolds number values and magnetic field intensity, resulting in a significant enhancement in heat transfer performance as the Hartman number increases. Higher Reynolds number result in expanded the velocity patterns and significant changes in temperature distribution within the cavity. Furthermore, the rate of heat exchange improves with the Reynolds number.

• The optimal conditions for achieving the highest heat transfer rate are as follows: Richardson number set to 0.1, volume fraction of particles (φ) at 4%, Hartman number (H_a) at 100, angle of inclination (γ) at 15°, and Reynolds number (R_e) greater than 700.

NOMENCLATURES

Symbols / Parameters

A, B: Dimensionless Heat block
C_p: Particular capacity for heat [$K^{-1}\times J\times Kg^{-1}$]
G : Acceleration due to gravity [$s^{-1}\times m^2$]
B_0: Magnetic_eld strength [T]
G_r: Grashof number
H : Characteristic length [m]
NU: Number of nusselt
K: Conductivity of heat [$W\times m^2\times K^{-1}$]
p : Pressure [Pa]
L : Heat blocklenght
P : Dimensionlesspressure
R_e : Reynoldsnumber
P_r : The number of Prandtl
$q"$: The Heat transfer [$m^{-2}\times W$]
Ri : The number of Richardson
T : Temperature (K)
X, Y, Z : Dimensionlesscoordinates
U, V, W : Dimensionless speed
α : Diffusion of heat [$s^{-1}\times m^2$]
φ : Solid volume fraction of nanoparticles
β : The Thermal expansion coefficient [K^{-1}]
σ : Effective electrical conductivity [$\Omega\times m^{-1}$]
μ : Dynamical viscosity [$s^{-1}\times kg\times m^{-1}$]
θ : Dimensionless temperature,
υ : Kinematical viscosity [$s^{-1}\times m^2$]
ρ : Density [$Kg\times m^{-3}$]
γ : Magnetic field inclination [°]
B : Bottom
C : Cold
F : Fluid
G : Global
H : Horizontal
M_f: Magnetic_field
Hnf : Hybrid-nanofluid

REFERENCES

[1] A. Asadi, M. Rezaniakolaei, A.R. Lasse, "Heat Transfer Efficiency of Al_2O_3 MWCNT/Thermal Oil Hybrid Nanofluid as a Cooling Fluid in Thermal and Energy Management Applications: An Experimental and Theoretical Investigation", Int. J. Heat Mass. Transf., Vol. 117, pp. 474-486, 2018.

[2] A.M. Rashad, T. Armaghani, et al., "Entropy Generation and MHD Natural Convection of a Nanofluid in an Inclined Square Porous Cavity: Effects of a Heat Sink and Source Size and Location", Chinese Journal of Physics, Vol. 56, pp. 193-211, 2018.

[3] A. Maanser, A. Benouis, M. Gherdoui, R. Boudjadja, "Effect of Temperature on Mechanical Properties of Mortars with Incorporation of Different Chemical Admixtures", International Journal on Technical and Physical Problems of Engineering (IJTPE), Issue 51, Vol. 14, No. 2, pp. 330-338, June 2022.

[4] K. Mehmood, S. Hussain, M. Sagheer, "Numerical Simulation of MHD Mixed Convection in Alumina-Water Nanofluid Filled Square Porous Cavity Using KKL Model: Effects of Non-Linear Thermal Radiation and Inclined Magnetic Field", Journal of Molecular Liquids, Vol. 238, pp. 485-498, 2017.

[5] H.R. Ashorynejad, A. Shahriari, "MHD Natural Convection of Hybrid Nanofluid in an Open Wavy Cavity", Results Phys., Vol. 9, pp. 440-455, 2018.

[6] R. Alizadeh, et al., "Machine-Learning Enhanced Analysis of Mixed Biothermal Convection of Single Particle and Hybrid Nanofluids Within a Complex Configuration", Ind. Eng. Chem. Res., 2021.

[7] A.H. Pordanjani, et al., "Effect of Magnetic Field on Mixed Convection and Entropy Generation of Hybrid Nanofluid in an Inclined Enclosure: Sensitivity Analysis and Optimization", Eur. Phys. J. Plus, Vol. 134, No. 8, p. 412, 2019.

[8] H. Chekenbah, A. El Abderrahmani, A. Aghanim, Y. Maataoui, R. Lasri, "Solving Problem of Partial Shading Condition in a Photovoltaic System Through a Self-Adaptive Fuzzy Logic Controller", International Journal on Technical and Physical Problems of Engineering (IJTPE), Issue 47, Vol. 13, No. 2, pp. 130-137, June 2021.

[9] K. Bouzid, L. Belarche, I. Abourida, et al., "Numerical Investigation of Mixed Convection Inside a Three-Dimensional l-Shaped Cavity Filled with Hybrid-Nanofluids in the Presence of a Heating Block", Thermal Science International Scientific Journal, p. 57, 2024.

[10] T. Tayebi, A.J. Chamkha, "Entropy Generation Analysis due to MHD Natural Convection Flow in a Cavity Occupied with Hybrid Nanofluid and Equipped with a Conducting Hollow Cylinder", J. Therm. Anal. Calorim., Vol. 139, Issue 3, pp. 2165-2179, 2020.

[11] M. Ghalambaz, S.A. Mehryan, E. Izadpanahi, A.J. Chamkha, D. Wen, "MHD Natural Convection of Cu–Al_2O_3 Water Hybrid Nanofluids in a Cavity Equally Divided into Two Parts by a Vertical Flexible Partition Membrane", J. Therm. Anal. Calorim, Vol. 138, No. 2, pp. 1723-1743, 2019.

[12] F. Fadaei, M. Shahrokhi, A. Molaei Dehkordi, Z. Abbasi, "Heat Transfer Enhancement of Fe_3O_4 Ferrofluids in the Presence of Magnetic Field", J. Magn. Magn. Mater, Vol. 429, pp. 314-323, 2017.

[13] M.A. Teamah, "Numerical Simulation of Double Diffusive Natural Convection in Rectangular Enclosure in the Presences of Magnetic Field and Heat Source", Int. J. Therm. Sci., Vol. 47, No. 3, pp. 237-248, 2008.

[14] M.A. Teamah, A.F. Elsafty, et al., "Massoud, Numerical Simulation of Double-Diffusive Natural Convective Flow in an Inclined Rectangular Enclosure in the Presence of Magnetic Field and Heat Source", Int. J. Therm. Sci., Vol. 52, No. 1, pp. 161-175, 2012.
[15] H.F. Oztop, K. Al Salem, I. Pop, "MHD Mixed Convection in Alid-Driven Cavity with Corner Heater", Int. J. Heat Mass Transf., Vol. 54, pp. 15-16, pp. 3494-3504, 2011.
[16] S. Hussain, S.E. Ahmed, T. Akbar, "Entropy Generation Analysis in MHD Mixed Convection of HNF in an Open Cavity with a Horizontal Channel Containing an Adiabatic Obstacle", Int. J. Heat Mass Tran., Vol. 114, pp. 1054-1066, 2017.
[17] A. Asadi, A. Hossein Nezhad, F. Sarhaddi, T. Keykha, "Laminar Ferrofluid Heat Transfer in Presence of Non-Uniform Magnetic Field in a Channel with Sinusoidal Wall: A Numerical Study", J. Magn. Magn. Mater., Vol. 471, pp. 56-63, 2019.
[18] G.H.R. Kefayati, "FDLBM Simulation of Magnetic Field Effect on Non-Newtonian Blood Flow in a Cavity Driven by the Motion of Two Facing Lids", Powder Technol., Vol. 253, pp. 325-337, 2014.
[19] W. Aich, L. Kolsi, M.N. Borjini, A.A. Al Rashed, H.B. Aissia, H.F. Oztop, N. Abu Hamdeh, "Three-Dimensional Computational Fluid Dynamics Analysis of Buoyancy-Driven Natural Ventilation and Entropy Generation in a Prismatic Green House", Therm. Sci., Vol. 22, No. 1, Part A, pp. 73-85, 2018.
[20] K. Al Salem, H.F. Oztop, I. Pop, Y. Varol, "Effects of Moving Liddirection on MHD Mixed Convection in a Linearly Heated Cavity", Int. J. Heat Mass Transf., Vol. 55, No. 4, pp. 1103-1112, 2012.
[21] B. Ghorbani, S. Ebrahimi, K. Vijayaghavan, "CFD Modeling and Sensitivity Analysis of Heat Transfer Enhancement of a Ferrofluid Flow in the Presence of a Magnetic Field", Int. J. Heat Mass Transf., Vol. 127, Part A, pp. 544-552, December 2018.
[22] T. Armaghani, M.S. Sadeghi, A.M. Rashad, M.A. Mansour, A.J. Chamkha, A.S. Dogonchi, H.A. Nabwey, "MHD Mixed Convection of Localized Heat Source/Sink in an Al_2O_3-Cu/Water Hybrid Nanofluid in L-Shaped Cavity", Alexandria Engineering Journal, Vol. 60, pp. 2947-2962, 2021.
[23] Z. Mehrez, A. El Cafsi, "Forced convection Fe_3O_4/Water Nanofluid Flow Through a Horizontal Channel under the Influence of a Non-Uniform Magnetic Field", Eur. Phys. J. Plus., pp. 136-451, 2021.
[24] S.V. Patankar, "Numerical Heat Transfer and Fluid Flow", McGraw-Hill, New York, USA, 1980.
[25] J. Ravnik, "Analysis of Three-Dimensional Natural Convection of Nanofluids by BEM", Engineering Analysis with Boundary Elements, Vol. 34, No. 12, pp. 1018-1030, 2010.
[26] N.O. Moraga, S.E. Lopez, "Numerical Simulation of Three-Dimensional Mixed Convection in an Air-Cooled Cavity", Numerical Heat Transfer, Part A: Applications, Vol. 45, No. 8, pp. 811-824, 2004.
[27] R.S.R. Gorla, S. Siddiqa, M.A. Rashad, T. Salah, "Heat Source/ Sink Effects on a Hybrid Nanofluid-Filled Porous Cavity", J. Thermophys. Heat Transf., Vol. 31, No. 4, pp. 847-857, 2017.
[28] H. Doghmi, I. Abourida, L. Belarche, et al., "Numerical Study of Mixed Convection Inside a Three-Dimensional Ventilated Cavity in the Presence of an Isothermal Heating Block", International Journal of Heat and Technology, Vol. 36, No. 2, pp. 447-456, 2018.

BIOGRAPHIES

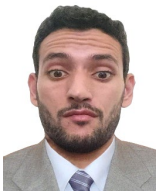

Name: **Kamal**
Surname: **Bouzid**
Birthday: 25.12.1992
Birthplace: Ouarzazate, Morocco
Bachelor: Mechanical Engineering, Industrial Product Design, ENSET, Mohamed V University, Rabat, Morocco, 2014
Master: Mechanics, Mechanical Engineering, ENSET, Mohamed V University, Rabat, Morocco, 2016
Doctorate: Student, Mechanics, Processes, Energy and Environement, Natural and Mixed Convection within Basic and Elaborate Enclosures, LMPEE, Faculty of UIZ, National School of Applied Science (ENSA), Agadir, Morocco, Since 2019
The Last Scientific Position: Lecturer, Industrial and Mechanical Engineering, Ministry of Education and Sport, Agadir, Morocco, Since 2018
Research Interests: Mechanical Engineering, Heat and Mass Transfer, Production Process Optimization
Scientific Publications: 2 Papers, 1 Book, 1 Project

Name: **Lahoucine**
Surname: **Belarche**
Birthday: 27.03.1968
Birthplace: Tiznit, Morocco
Bachelor: Mechanical Engineering, ENSET, University Mohamed V, Rabat, Morocco, 2008
Master: Energy, Process and Energy Engineering, National School of Applied Science (ENSA), Ibn Zohr University, Agadir, Morocco, 2010
Doctorate: Energy, Fluid Mechanics, Energetics, and Thermo-Dynamics, National School of Applied Science (ENSA), Ibn Zohr University, Agadir, Morocco, 2015
The Last Scientific Position: Prof., Mechanical Engineering, Department of Mecanics, Processes, Energy and Environement, National School of Applied Science (ENSA), Ibn Zohr University, Agadir, Morocco, Since 2017
Research Interests: Heat and Mass Transfer and its Application in Mechanical and Industrial Engineering, Cooling of Electronics and Mechanical Components, Drying Technologies, Solar Collectors
Scientific Publications: 22 Papers, 2 Books, 5 Projects, 1 Thesis

Name: **Btissam**
Surname: **Abourida**
Birthday: 05.12.1974
Birthplace: Marrakesh, Morocco
Bachelor: Physics, Energy and Fluid Mechanics, Faculty of Sciences, Cadi Ayyad University, Marrakech, Morocco, 1993
Master: Physics, Energy and Fluid mechanics, Faculty of Sciences, Cadi Ayyad University, Marrakech, Morocco, 1995
Doctorate: Physics, Energy and Fluid Mechanics, Faculty of Sciences, Cadi Ayyad University, Marrakech, Morocco, 1999
The Last Scientific Position: Prof., Mechanics and Energy, Faculty of Sciences, Cadi Ayyad University, Marrakech, Morocco, Since 2020
Research Interests: Heat and Mass Transfer, and Energy
Scientific Publications: 24 Papers, 10 Books, 5 Projects, 1 Thesis

Name: **Ali**
Surname: **Siadi**
Birthday: 15.12.1970
Birthplace: Errachidia, Morocco
Bachelor: Physics and Electronics, Mohamed V University, Rabat, Morocco, 1994
Master: Energy, Process and Energy Engineering, National School of Applied Science (ENSA), Ibn Zohr University, Agadir, Morocco, 2011
Doctorate: Student, Energy, Fluid Mechanics, Energetics, and Thermo-dynamics, National School of Applied Science (ENSA), Ibn Zohr University, Agadir, Morocco, Since 2019
The Last Scientific Position: Chief Engineer CRMEF, Taroudant, Morocco, Since 1995
Research Interests: Computational Study and Investigation of Diverse 3D Flow Patterns: Laminar and Turbulent Flow Behaviors with Nanofluids in Ventilated Enclosures
Scientific Publications: 5 Papers, 2 Books, 1 Project